Role of a secondary coordination sphere residue in halogenation catalysis of non-heme iron enzymes

*R. Hunter Wilson, Sourav Chatterjee, Elizabeth R. Smithwick, Joseph J. Dalluge, Ambika Bhagi-Damodaran**

Department of Chemistry, University of Minnesota, Twin Cities, Minneapolis, MN 55455, USA

KEYWORDS. halogenation, DOPA, non-heme iron, 2OG-dependent, O_2 activation

ABSTRACT. Chemo- and regio-selective catalysis of C(sp^3)-H halogenation reaction is a formidable goal in chemical synthesis. 2-oxo-glutarate (2OG) dependent non-heme iron halogenases catalyze selective chlorination/bromination of C-H bonds and exhibit high sequence and structural similarities with non-heme iron hydroxylases. How the secondary coordination sphere (SCS) of these two enzyme systems differentiate and determine their reactivity is not understood. In this work, we show that tyrosine placement in the SCS of non-heme iron halogenases have a huge impact on their structure, function, and reactivity. We discover that a tyrosine mutant (F121Y) in SyrB2 halogenase undergoes post-translational oxidation to dihydroxyphenylalanine (DOPA) physiologically. A combination of spectroscopic, mass-spectrometric, and biochemical studies show that the DOPA modification in SyrB2 renders the enzyme non-functional. Further bioinformatics analysis suggests that halogenases, unlike hydroxylases, have a conserved placement of phenylalanine at position 121 to preclude such

unproductive oxidation. Overall, this study demonstrates the importance of the SCS in controlling the structure and enzymatic activity of non-heme iron halogenases. Our results will have significant implications towards the design of small-molecule and protein-based halogenation catalysts.

Introduction

2OG-dependent non-heme iron enzymes (NH-Fe) catalyze a diverse range of reactions ranging from epoxidation to stereo-inversion.[1] From natural product biosynthesis to cellular signaling and metabolism, the reactions catalyzed by this superfamily of enzymes serve crucial roles biologically.[2,3] Two subgroups of this superfamily are the hydroxylases and halogenases. Hydroxylases catalyze the insertion of a hydroxyl functional group into unactivated aliphatic C-H bonds while halogenases catalyze the insertion of a chloride/bromide functionality into such bonds. The difference in reactivity of the two enzymes is enabled by differences in their iron-binding primary coordination sphere. Hydroxylases bind iron via a 2 His/1 Carboxyl (Asp/Glu) facial triad analogous to halogenases except that in halogenases the carboxyl ligand is replaced by a non-polar Ala or Gly residue.[1,4] This amino acid substitution in halogenases enables the steric and electrostatic accommodation of an iron coordinated halide anion that is essential for halogenation reactivity.[5] Both hydroxylases and halogenases have been suggested to operate via a similar catalytic mechanism (**Fig S1**).[6,7] Once 2OG, iron, and substrate are bound to the enzyme, a conformational change is triggered that facilitates molecular oxygen binding to the iron center. Next, oxidative decarboxylation of the 2OG co-substrate results in the cleavage of oxygen's O-O bond and the formation of a high-valent ferryl intermediate (Fe^{IV}=O). The ferryl intermediate abstracts a hydrogen atom from the substrate, resulting in a ferric-hydroxyl (Fe^{III}-

OH) species and a substrate radical. At this point, the mechanisms for the hydroxylases and halogenases diverge. In hydroxylases, the hydroxyl group bound to the iron will "rebound" and combine with the substrate radical to give a hydroxylated product. In halogenases, the protein positions the halide ligand closer to the substrate radical than the hydroxyl ligand. This favors radical combination with the halide ligand resulting in a halogenated product, though a minor hydroxylated product is also possible through hydroxyl rebound.

This work focuses on a well-characterized halogenase, SyrB2, which chlorinates/brominates the side chain methyl group of its substrate Thr.[8,9] Amino acid Thr is delivered to the active site of SyrB2 via partner protein SyrB1's covalently attached phosphopantetheine (Ppt) group.[8] When Thr is substituted with non-native amino acid substrates like alpha-aminobutyric acid or norvaline, SyrB2 primarily hydroxylates them.[10] These studies and others have demonstrated the importance of SyrB2's interaction with Thr and other amino acid substrates to influence halogenation/hydroxylation reaction outcomes.[10–15] While substrate-protein interactions are well-understood, it's unclear how iron's secondary coordination sphere (SCS; amino acid residues that interact with the ligands bound to iron) governs reaction outcome in SyrB2 and other halogenases. From a broader perspective, while the impact of the SCS on the structure and function of heme iron enzymes have been extensively studied, little is known about how non-heme iron enzymes utilize SCS to control their reactivity.[16–20] In this work, we investigate the importance of iron's SCS in controlling SyrB2 halogenase's reactivity. Specifically, we establish the role of a hydrophobic Phe121 residue that is ~4 Å away from iron's chloride ligand towards configuring halogenase activity in SyrB2. Mutating this residue to Tyr facilitates its intracellular post-translational modification to a dihydroxyphenylalanine (DOPA) residue that renders SyrB2 non-functional. Beyond SyrB2, the F121 residue is highly conserved in halogenases, unlike

hydroxylases, signifying the differential nature of the SCS in the two enzyme classes. Overall, our studies emphasize the importance of the SCS in controlling catalytic activities of non-heme iron enzymes, particularly halogenases and hydroxylases.

Materials and Methods

Plasmid Design and Mutagenesis

SyrB1, SyrB2, SyrB2 mutants, and Sfp were all incorporated into pET-28a(+) vectors; TycF was incorporated into a pET-30b(+) vector. All plasmids are designed with a N-terminal His_6-Tag. Site directed mutagenesis was performed on the SyrB2 plasmid to form the F104Y and F121Y mutations using the Phusion™ Site Directed Mutagenesis Kit from Thermo Scientific. The forward and reverse primers (5' to 3') for the F104 mutation were: GAGTTCTATCCCAAATATCCGGGCG and TTTGGGATAGAACTCGGTACGCCAG respectively. The forward and reverse primers (5' to 3') for the F121Y mutation were: CACCTACGCCAATGCCTCCGGCA and CATTGGCGAAGGTGTCGGCCTGG respectively. A three-step denaturation, annealing, and extension protocol was used for both mutants with an annealing temperature of 67.6°C for F104 and 72.0°C for F121Y. All PCR experiments were performed using a Axygen Maxygene II instrument. All PCR products were transformed into DH5α cells (Thermo Scientific) for plasmid expression. Single mutant DNA sequences were confirmed using Sanger Sequencing at the UMN Genomics Center.

Protein Expression

SyrB1, SyrB2, SyrB2 mutants, and Sfp were all expressed using the same method. Plasmids containing the proteins were transformed into BL21(DE3) cells (Thermo Scientific) for protein overexpression. An overnight culture (~50 mL 2XYT broth, 0.05 mg/mL kanamycin) was grown at 37°C for ~16 hours at 220 RPM. Ten mL of the overnight culture was used to inoculate 1 L cultures (2XYT, 0.05 mg/L kanamycin) in 2.8L baffled flasks. A single drop of Antifoam 204 (Sigma) was added to each culture to aid in oxygen diffusion. Cultures were grown at 37°C until an OD_{600} of 0.6-0.8 was reached. Cultures were then placed in an ice bath for 15-20 minutes to cool. Isopropyl β-D-1-thiogalactopyranoside (IPTG, GoldBio) was add ed to a final concentration of 0.2 mM to induce protein overexpression. After 18 hrs of shaking at 18°C, cell pellets were harvested by centrifugation, flash frozen in liquid nitrogen, and stored at -20°C. Typical yields were ~8-10 g cell pellet/L culture. Overexpression for TycF followed the same protocol except the [IPTG] = 1 mM and the expression time was 72 hours.

Protein Purification

All buffers and solutions described herein were prepared in MilliQ water from a Barnstead GenPure water filtration system (Thermo Scientific) with a resistivity of at least 18.2 MΩ. For all proteins, thawed cell pellets were resuspended in 5 mL wash buffer/g of cells (wash buffer = 50 mM HEPES (Sigma: Biocertified), 300 mM NaCl (Sigma: BioUltra), 5 mM imidazole (Sigma: ReagentPlus), pH = 7.5). Resuspension was supplemented with Pierce™ Protease Inhibitor, EDTA-free tablets (Thermo Scientific). After resuspension, cells were lysed by sonication and centrifuged to remove any non-soluble cell debris (20,000 RPM, 20 min, 4°C). Supernatant was filtered with 0.43 micron syringe filters and loaded onto a wash-buffer

equilibrated 5 mL HisTrapFF column (Cytiva, 2 mL/min binding rate) using an AKTA Start protein purification system (Cytiva). After sample application, the column was washed with 15 CV of wash buffer to elute any non-specific binding proteins. Elution occurred using a linear gradient from 0% to 100% elution buffer (elution buffer = 50 mM HEPES, 100 mM NaCl, 250 mM imidazole, pH = 7.5). For TycF, an isocratic elution was performed by washing the column with 10 CV of 30% elution buffer then 10 CV of 100% elution buffer. Relevant protein fractions, as determined by SDS-PAGE analysis, were pooled. Sfp and TycF were dialyzed against RXN buffer (20 mM HEPES, pH =7.5) overnight, filtered, concentrated using Amicon™ Ultra 10 kDa MWCO centrifugal filter units (Millipore Sigma), flash frozen in liquid nitrogen, and stored at -80°C.

SyrB2 and its mutants were buffer exchanged into RXN buffer three times using Amicon™ Ultra 30 kDa MWCO centrifugal filter units (Millipore Sigma) after initial immobilized metal affinity chromatography. Concentrated protein was diluted to ~8 mL with RXN buffer and filtered with 0.22-micron filters prior to loading into a superloop connected to an AKTA Pure protein purification system (Cytiva) for size-exclusion chromatography. A HiLoad 26/600 Superdex 200 pg column (Cytiva) was pre-equilibrated with RXN buffer. Protein was then applied and eluted (flow = 1 mL/min) over three injection/elution cycles. Relevant fractions, as determined by SDS-PAGE, were pooled and concentrated in the Amicon™ Ultra 30 kDa MWCO centrifugal filter units. Protein was aliquoted, flash frozen in liquid nitrogen, and stored at -80°C until further use. Preparation of SyrB1 after initial immobilized metal affinity chromatography protein is described in the next section. All protein concentrations were determined using the absorbance at 280 nm using molar extinction coefficients from the ProtParam tool.[21]

Ppt and Thr attachment to SyrB1

After immobilized metal affinity chromatography, SyrB1 was buffer exchanged into RXN buffer three times using Amicon™ Ultra 50 kDa MWCO centrifugal filter units (Millipore Sigma). To attach the Ppt cofactor, SyrB1 (100 μM) was incubated with coenzyme A (1 mM, Sigma: cofactor for acyl transfer), $MgSO_4$ (5 mM, Sigma: BioReagent), and phosphopantetheinyl transferase Sfp (5 μM) for 90 minutes at room temperature. The reaction mixture was concentrated using the same centrifugal filter units and then diluted to ~8 mL with reaction buffer. After filtering, the protein was loaded into the superloop of an AKTA Pure protein purification system. The same elution method as described for the SyrB2 proteins was performed except that the flow rate was adjusted to 0.8 mL/min.

Relevant fractions from size-exclusion chromatography were pooled and concentrated using centrifugal filter units. To append threonine to the protein, SyrB1-Ppt (100 μM) was incubated with $MgSO_4$ (5 mM), ATP (10 mM, Sigma: Grade I, ≥99%, from microbial), and L-threonine (10 mM, Sigma: reagent grade, ≥98% (HPLC)) in RXN buffer for 30 min at room temperature. After this step, it's crucial that SyrB1-Ppt-Thr remain at cool temperatures to prevent spontaneous hydrolysis of the thioester bond that links threonine to PPT-SyrB1. The amino acid-loaded protein was then concentrated using the previous centrifugal filter unit, and buffer exchanged four times with RXN buffer to remove excess reaction components. The protein was aliquoted, flash frozen in liquid nitrogen, and stored at -80°C.

UV-Vis measurements

All UV-Vis measurements were recorded on either a Cary 8454 UV-Vis Spectrophotometer or Cary 4000 UV-Vis Spectrophotometer. Measurements with the Cary 4000 were performed in

double beam mode with a *S/N* ratio of 10000, a timeout of 0.2 s, and a spectral bandwidth of 2 nm. All spectra were background corrected at 900 nm.

EPR measurements

All SyrB2 samples (WT and F121Y/DOPA) were prepared at a final concentration of 450 μM in a volume of 280 μL. Samples were transferred to EPR Tubes (Wilmad) and frozen in a methanol/dry ice bath followed by a liquid nitrogen bath. Both samples were stored in a liquid nitrogen dewar until use. EPR measurements were performed on a Bruker Elexsys E-500 spectrometer with an E500-T-DU Digital upgrade equipped with an Oxford ESR-910 liquid He cryostat. EPR collection parameters for F121Y/DOPA SyrB2 are : microwave frequency = 9.6 GHz; microwave power = 1.69 mW, modulation amplitude = 9 G, modulation frequency = 100 kHz, temperature = 2 K. EPR collection parameters for WT SyrB2 were: microwave frequency = 9.6 GHz, microwave power = 210 μW, modulation amplitude = 5 G, modulation frequency = 100 kHz, temperature = 2 K.

DOPA nitration/oxidation reaction assay

The following procedure was adapted from the method of Waite et al.[22] Fresh denaturing sodium acetate buffer (200 mM, 8 M urea (Sigma: BioUltra), pH = 4.5) was prepared. SyrB2-F121Y/DOPA protein was diluted and buffer exchanged into this denaturing buffer three times to remove HEPES. Another solution of 1.41 M $NaNO_2$/0.41 M Na_2MoO_4 (nitration reagent, both Sigma: ACS Reagent) was prepared in MilliQ water. The denatured SyrB2-F121Y/DOPA protein (300 μL) was mixed with 1 equivalent (v/v) of the nitration reagent forming a yellow-colored solution. 1 M NaOH (400 μL) was immediately added to oxidize the nitrated species and

form the pink-colored dinitro-quinone complex. The UV-Vis spectrum of the reaction was then recorded on a Cary 4000 instrument using the parameters described above.

Native Protein Mass Spectrometry

A fresh solution of 5 mM ammonium acetate, pH = 6.5 (AA, Mallinckrodt: Analytical Reagent) was prepared in MilliQ water. Both the WT SyrB2 and F121Y/DOPA SyrB2 were buffer exchanged four times into AA using prewashed (100 mM NaOH then AA) 0.5 mL Amicon™ Ultra 30 kDa MWCO centrifugal filter units (Millipore Sigma). Mass spectral analysis of intact SyrB2 protein(s) in their native state was achieved by direct infusion of aqueous buffer-exchanged solutions of SyrB2 (50 μM protein, 50 μM aqueous NH_4OAc diluted with LC/MS grade water) into a Waters Synapt G2 quadrupole time-of-flight mass spectrometer employing the following instrumental parameters: capillary voltage, 3.0; cone voltage, 30; extraction cone voltage: 5.0; source temperature, 100 °C; desolvation temperature, 350°C; cone gas flow (L/h): 20; desolvation gas flow (L/h), 440. Samples were infused at 10 μL/min and mass spectra were acquired in continuum mode over the range *m/z* 1000 to *m/z* 3000 with a 0.5 s scan time with the following manual quadrupole profile: mass 1000, dwell time 10, ramp time 20; mass 2000, dwell time 20, ramp time 50; mass 2500. Mass spectra of intact (native state) proteins were deconvoluted employing the Waters MaxEnt 1 algorithm with the Waters Masslynx® operating system.

Halogenation Assays

SyrB2 or SyrB2-F121Y/DOPA (100 μM) was added to RXN buffer containing NaCl (10 mM), 2OG (1 mM). For the WT system, ferrous ammonium sulfate (Sigma: BioUltra, in 2.5 mM H_2SO_4) was added to the reaction, and the solution was pipette mixed. SyrB1-PPT-Thr was

added to the rxn to a final concentration of 100 μM, and the rxn was pipette mixed again. The total reaction volume was 200 μL, and all steps so far were performed on ice. One volume equivalent of O_2 saturated buffer was added to the reaction, and each solution was pipette mixed. All reactions were transferred to an Eppendorf Thermomixer® and spun at 300 RPM for 10 minutes and were then transferred to ice. The reactions were loaded into pre-washed (100 mM NaOH then RXN buffer) 0.5 mL Amicon™ Ultra 10 kDa MWCO centrifugal filter units, concentrated to ~50 μL, then diluted to 500 μL, and concentrated again. This washing step was performed two more times. All centrifugation steps occurred at 4°C to prevent thioester cleavage. TycF thioesterase (final concentration of 5 μM) was added to each centricon for product cleavage in a final volume of 150 μL. The product cleavage reaction was run for 90 minutes at 25°C. The centricon volume was diluted to 400 μL with RXN buffer and the flow-through was collected into deactivated, silanized Waters vials. Three total rounds of dilution and collection were performed to collect all cleaved product. The vials containing ~1.2 mL of cleaved product in RXN buffer were lyophilized overnight.

Dry product was reconstituted in 160 μL of 100 mM borate buffer (Ricca: Analytical Grade); 18.5 μL of MilliQ H_2O & 1.5 μL of 5 M NaOH was added to each solution to bring the final pH to 8.5. Derivatization agent, 6-aminoquinolyl-N-hydroxysuccinimidyl carbamate (160 mM in acetonitrile, AQC, Cayman Chemical) was added to a final concentration of 6 mM and a total reaction volume of 200 μL. Reactions were mixed and incubated at room temperature for 10 minutes.

A Waters Acquity UPLC coupled to a Waters triple quadrupole mass spectrometer (Acquity TQD) was used for chromatographic separation and detection of AQC-derivatized amino acids. A Waters CORTECS UPLC C18 column (2.1 mm x 100 mm x1.6 μm) at 55 °C was used during

the following 10 min gradient separation with A: Water (VWR International, Omnisolv LC/MS grade) containing 0.1% formic acid and B: ACN (VWR International, Omnisolv LC/MS grade) containing 0.1% formic acid as two mobile phases at a flow rate of 0.5 mL/min: 1% B, 0 min to 1.0 min; 1% B to 13% B, 1.0 min to 2.0 min; 13% B to 15% B, 2.0 min to 5.5 min; 15%B to 95% B, 5.5. min to 6.5 min; 95% B, 6.5 min to 7.5 min; 95% B to 1% B, 7.5 min to 7.7 min; 1% B, 7.7 min to 10 min. The SRM transitions monitored for each analyte are tabulated in Table S1. Dwell time for each transition was 0.01 s. For electrospray ionization tandem mass spectrometry (ESI-MS/MS) in positive ionization mode, parameters were as follows: capillary, 3.5 kV; cone, 35.0 V; extractor, 3 V; rf lens, 0.3 V; source temperature, 120 °C; desolvation temperature, 350 °C; desolvation flow, 800 L/h; cone gas flow, 20 L/h; low-mass resolution (Q1), 15 V; high-mass resolution (Q1), 15 V; ion energy (Q1), 0.3 V; entrance -5 V; exit, 1 V; collision energies listed in Table S1; low-mass resolution (Q2), 15 V; high-mass resolution (Q2), 15 V; ion energy (Q2) 3.5 V.

Bioinformatics Analysis

To observe the sequence conservation position 121, the amino acid sequence for SyrB2 was used as a query for a BLAST search in the non-redundant protein database with a e^{-5} cutoff, resulting in 846 hits. Sequences were aligned using the MUSCLE algorithm and visualized using the AliView software. Results were filtered between the halogenases (HXA/G motif, 186 sequences) and hydroxylases (HXD/E motif, 660 sequences). Each of the sequence groups were subjected to cluster analysis using the CD-HIT web server to remove redundant sequences of 90% similarity (resulting in 132 halogenase sequences and 503 hydroxylase sequences). Individual halogenase/hydroxylase sequences were realigned with MUSCLE. LOGOS plots were generated for each cluster using WebLogo (https://weblogo.berkeley.edu/logo.cgi).

Results and Discussion

Observation and characterization of DOPA post-translational modification in F121Y SyrB2 variant

A visual inspection of SyrB2's active site reveals two hydrophobic Phe residues that were ~4 Å away from iron's ligands (**Fig. 1A**).[5] Specifically, the F104 residue is 3.8 Å from a water ligand and F121 residue is 3.9 Å away from the chloride ligand. To assess if the hydrophobic nature of these residues was important, tyrosine mutants of both residues, i.e. F104Y and F121Y SyrB2, were constructed, expressed, and purified. Upon purification, WT SyrB2 and F104Y exhibited no signatures in the visible range of the UV-Vis spectrum, implying that both halogenases purify without iron bound to the active site (**Fig. 1B**). In contrast, SyrB2-F121Y purified as a blue-green solution with a λ_{max} at 650 nm (**Fig 1B**). This blue-green chromophore has been observed in a few NHFe proteins previously, and has been postulated to originate from a ligand-to-metal charge transfer band (LMCT) of a DOPA-Fe^{3+} species.[23–27] We hypothesize that such a species has formed from intra-cellular oxidation of the F121Y mutant and will refer to this SyrB2 variant as F121Y/DOPA.

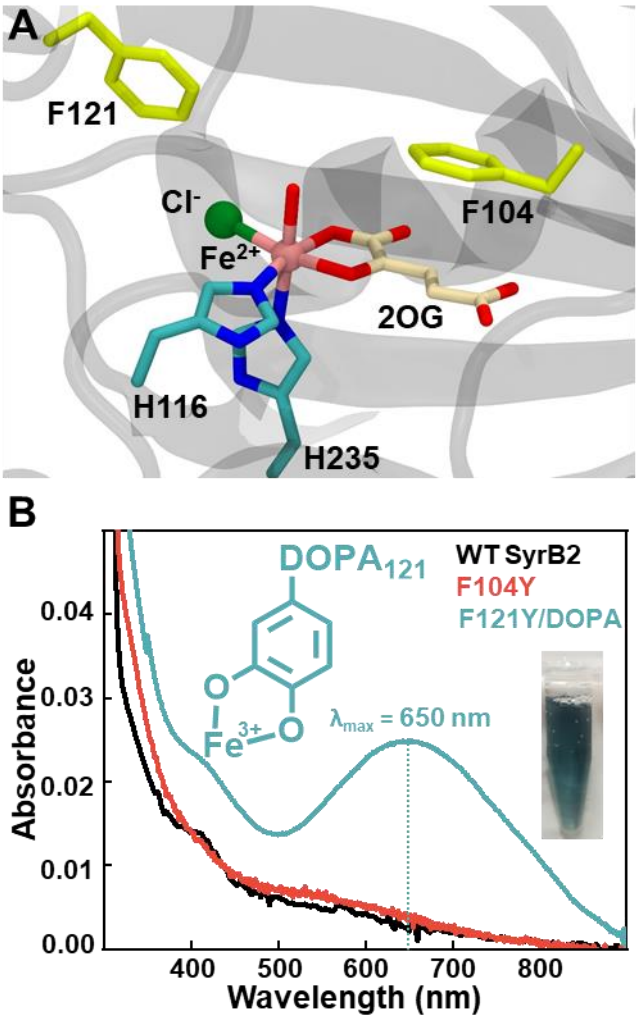

Figure 1. A) Crystal structure of SyrB2 halogenase (PDB: 2FCT). Prospective residues for mutation are highlighted in yellow. **B)** UV-vis spectra of purified SyrB2 WT and mutant proteins (100 μM). A blue-green chromophore is present in the F121Y/DOPA variant, consistent with DOPA incorporation. Shown in inset is the structure of ferric-DOPA and a picture of purified SyrB2-F121Y/DOPA protein.

To further investigate the iron oxidation state in F121Y/DOPA, we attempted to oxidize the protein using hydrogen peroxide (**Fig. S2**). Even after incubation with 100 equivalents of

peroxide, no shift in the LMCT band was observed, which implies that the iron center is not in the ferrous state. To further characterize the electronic structure of the iron center, we investigated the F121Y/DOPA protein with EPR spectroscopy. The X-band EPR spectrum shows a distinct signal at g ~ 4.29 with additional features at g ~ 5.03 and 9.06 (Fig 2A). The signal at g ~ 4.29 is a hallmark of high-spin ferric iron species in a highly orthorhombic environment (E/D = 0.33).[28–31] The broad shoulder at g ~ 5.03 and small peak at g ~ 9.06 could be originating from a different Fe^{3+}-bound species in a more rhombic environment (E/D = 0.2). A variation in coordination number of the ferric-DOPA species in F121Y/DOPA could explain the heterogeneity of species in the EPR spectrum. Nevertheless, no EPR signals are observed in the WT SyrB2 spectrum confirming the absence of ferric iron in this protein sample (**Fig 2A**).

While EPR spectroscopic studies confirm the presence of a high-spin ferric center in F121Y/DOPA sample, similar signals have been previously observed in a ferric-phenolate complex (i.e. a tyrosinate residue binding to Fe^{3+}) as well.[29] However, high-spin ferric-phenolate species exhibit UV signatures blue-shifted (550 nm) relative to the F121Y/DOPA species (**Fig 1B**).[28,29] To exclude the possibility of ferric-tyrosinate and confirm the presence of DOPA post-translational modification in F121Y/DOPA sample, we executed a reaction that specifically targets DOPA amino acids.[22] Nitration/oxidation of the DOPA amino acid results in the formation of a di-nitro-DOPA-quinone species with a distinct UV-Vis signature at 500 nm (**Fig. S3A**). We performed this reaction on different concentrations of L-DOPA free amino acid to develop a standard curve, which would quantify the extent of DOPA modification in F121Y/DOPA (**Fig. S3B**). After denaturation of F121Y/DOPA in acidic buffer, the nitration/oxidation reaction was performed, and the UV-Vis spectrum was recorded (**Fig 2B**). A peak at 510 nm was present in the product, consistent with other DOPA-proteins treated with this

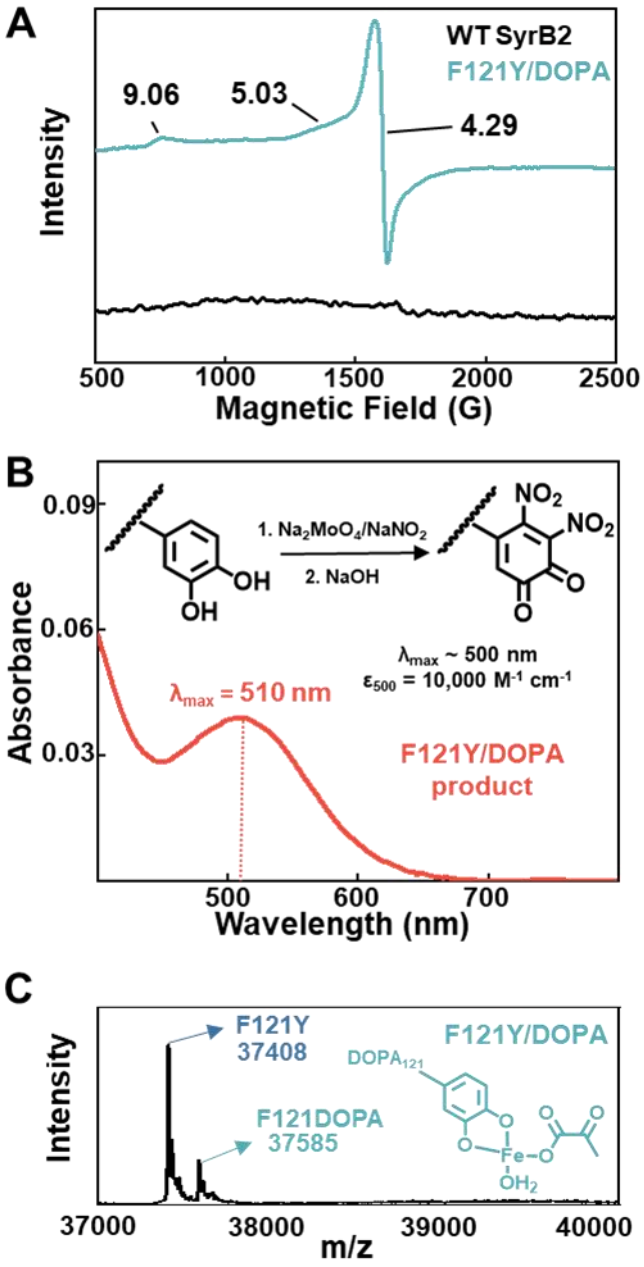

Figure 2. A) X-band EPR spectrum of purified WT SyrB2 and SyrB2-F121Y/DOPA. g-values are assigned for features in the F121Y/DOPA spectrum **B)** UV-Vis spectrum of a DOPA-specific nitration/oxidation reaction product on 20 μM SyrB2-F121Y/DOPA supports ~20% DOPA incorporation into SyrB2. **C)** Deconvoluted Native Mass Spectrum of the SyrB2-F121Y/DOPA

protein mixture. Two species are observed in the mixture: apo SyrB2-F121Y and SyrB2-F121DOPA with iron and pyruvate bound.

method, supporting DOPA modification in F121Y/DOPA SyrB2. Based on the absorbance values (0.04, $\varepsilon_{500\ nm,\ L\text{-}DOPA}$ = 9,800 M^{-1} cm^{-1}), ~20% of the F121Y/DOPA protein mixture contains the DOPA modification. Thus, F121Y is not fully oxidized to F121DOPA during protein expression analogous to iron-substituted catechol dioxygenase and F208Y ribonucleotide reductase which also purified as a mixture of tyrosine and DOPA containing variants.[23,32] Oxidation of tyrosine to DOPA likely occurs through the formation of the ferryl intermediate. Both hydroxylases and halogenases have evolved to bind their substrates prior to forming the reactive ferryl oxidant.[1,7] Thus, any non-productive ferryl formation in the absence of native substrate likely occurs on a very slow timescale which could explain why only a fraction of F121Y/DOPA exhibits the DOPA modification.

To further characterize the DOPA species, we performed intact native protein mass spectrometry on F121Y/DOPA SyrB2. This analysis would reveal which ligands, if any, were bound in the proteins. Representative mass spectra of F121Y/DOPA SyrB2 is illustrated in **Fig S4**. Algorithmic deconvolution of these peaks reveal the masses of the intact SyrB2 F121Y/DOPA protein (**Fig 2C**). The first mass at 37408 Da corresponds to the apo SyrB2-F121Y mutant. This mass is lower than expected for F121Y SyrB2 (theoretical mass: 37525 Da). This missing mass (117 Da) can be accounted for by the C-terminal residue, valine, which was cleaved during ionization in the MS experiments. A second less intense peak was found at 37585 Da, which is 177 Da greater than the apo F121Y species. Given the presence of iron and DOPA modification accounts for only 72 Da of mass, an extra 105 Da is left unaccounted for. Since the binding of native ligands 2OG (144 Da) and succinate (116 Da) cannot account for this mass differential, other ligands may be present

bound to the ferric-DOPA active site. We propose that a non-native ligand, pyruvate (87 Da), is bound to ferric ion in the active site via its alpha-keto functional group.[29] The active site is possibly quite perturbed with the formation of the ferric-DOPA species (F121 is located ~6 Å from the iron center in the WT crystal structure) and it's feasible that the protein's affinity for various ligands has changed. Given the ubiquity of pyruvate in the cellular environment (390 μM), the over-expressed protein would have an abundance of this ligand available to bind.[33] The rest of the unaccounted mass (18 Da) is explained by an aqua ligand, which is present in the WT crystal structure and numerous other non-heme iron structures.[5] Overall, using a combination of spectroscopic, mass-spectrometric, and biochemical studies, we were able to confirm the formation of DOPA post-translational modification in SyrB2 halogenase.

DOPA modification in SyrB2 forms an off-cycle, catalytically inactive species

Next, we tested the impact of DOPA post-translational modification on the halogenation catalysis of SyrB2. To that end, we developed halogenation assays for SyrB2 with its native substrate, Thr, which is delivered to SyrB2's active site while covalently bound to the ppt group of SyrB1. Chlorinated, hydroxylated (minor product), or unreacted threonine were liberated from SyrB1 after incubation with TycF thioesterase.[34] These products were first derivatized with 6-aminoquinolyl-N-hydroxysuccinimidyl carbamate (AQC) and then analyzed by reversed-phase UPLC/Multiple-Reaction-Monitoring-MS/MS for detection. WT-SyrB2, when subjected to halogenation assay, reveals AQC-Cl-Thr as the major product, eluting slightly after the unreacted AQC-Thr (**Fig 3A**). Isotopic ratios of AQC-^{35}Cl-Thr to AQC-^{37}Cl-Thr were shown to be 3:1, consistent with the natural abundance of chlorine, and providing validation to the identity of chlorinated Thr (**Fig S5**). The AQC-OH-Thr minor product was also observed, eluting prior to the unreacted AQC-Thr, though with much less intensity than AQC-Cl-Thr. SyrB2-

F121Y/DOPA, on the other hand, when subjected to similar halogenation assays (with or without the reductant ascorbate), showed no chlorinated or hydroxylated products (**Fig 3B, S6-7**). The only analyte observed corresponds to the unreacted Thr substrate (**Fig 3B, Fig S6-7**). While a low-intensity peak is present close to the noise at 2.52 min. in the AQC-^{35}Cl-Thr channel, no such peak is seen at the same elution time in the AQC-^{37}Cl-Thr channel suggesting no chlorinated product was formed. Even in the presence of ten equivalents of ascorbate, no products were observed (**Fig S7**). With these observations, we postulate that the ferric-DOPA SyrB2 species is a catalytically inactive, off-cycle species. We hypothesize that the modification of tyrosine to DOPA itself isn't necessarily the reason why F121Y/DOPA is catalytically inactive. It's the binding of ferric iron by the catecholate group of DOPA that results in an enzymatic species that's not part of the overall catalytic cycle. The DOPA121 is possibly bound to the ferric iron in a bidentate fashion which would result in large distortions in the active site, since F121 is located ~6 Å away from iron in the WT active site. To test this hypothesis, we performed UV-Vis titration of chloride into SyrB2-F121Y/DOPA and observed no perturbation in the LMCT band eluding to the fact that DOPA121 residue is binding in a position where chloride would bind or that distortion of the active site prevents chloride binding (**Fig S8**). Furthermore, it's unclear whether both histidine ligands would still be bound to ferric iron, as they would be needed for proper iron positioning in the active site for native activity. Saturation of coordination sites by DOPA121 would also prevent cofactors like 2OG and oxygen from binding to the iron site. Occupancy of coordination sites by pyruvate, as shown in our MS

studies, would also exacerbate this problem. Overall, the sequestration of ferric iron by the modified DOPA residue abolishes any catalytic activity of SyrB2.

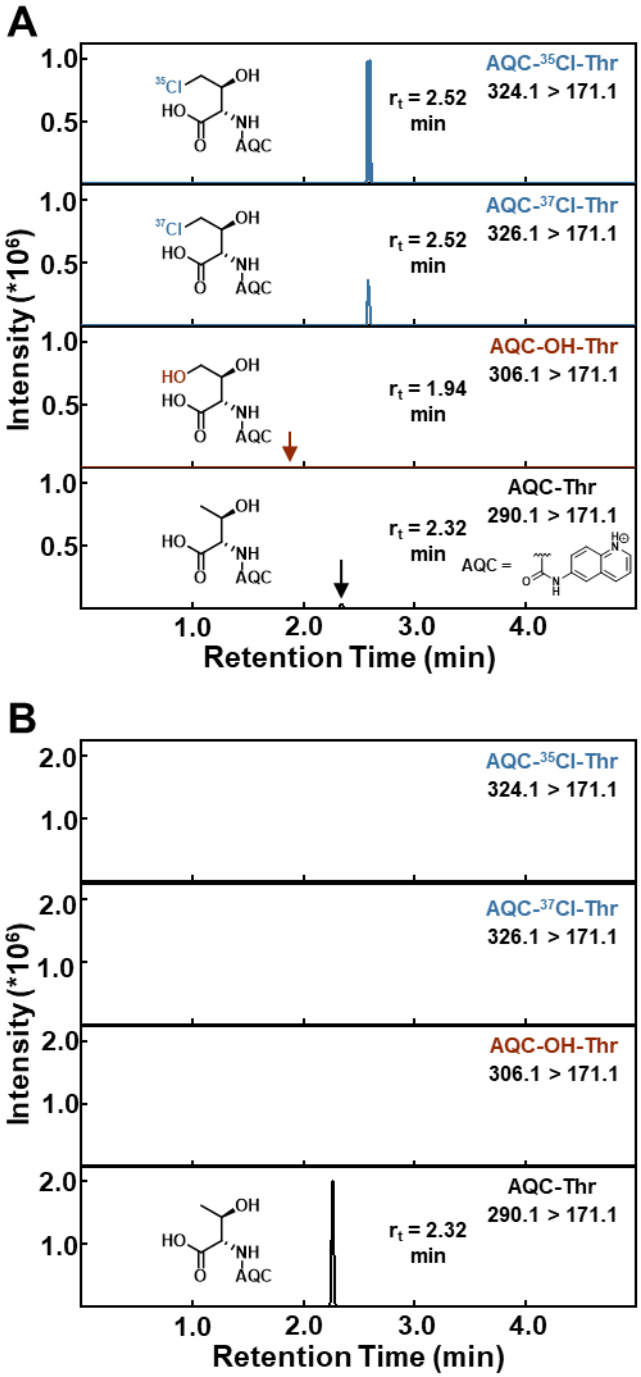

Figure 3. UPLC-MRM-MS/MS chromatograms of the halogenation reaction products for the **A)** WT and **B)** F121Y/DOPA SyrB2 proteins. Reactions using the F121Y/DOPA protein result in no

halogenated or hydroxylated products. Mass transitions for each unique analyte are given in the top right of each chromatogram.

Bioinformatic analysis reveals a conserved phenylalanine at position 121 in halogenases but not hydroxylases

While we've shown that F121 residue plays a significant role in preventing unproductive oxidation in SyrB2, we wanted to assess the impact of this residue across similar proteins. Using the SyrB2 sequence, we performed a BLAST analysis and sorted hits into hydroxylases (HXD/E motif) or halogenases (HXA/G motif). After removing redundant hits, 635 protein sequences were aligned, and LOGOS plots were generated (**Fig 4A**). For hydroxylases, the prominent amino acid in position 121 is a redox-active tyrosine. In halogenases, on the other hand, the redox-inactive phenylalanine is strongly conserved at position 121. Since mutation of phenylalanine to tyrosine at this position in SyrB2 has led to an off-cycle species, it's intriguing that the hydroxylases have evolved to have a redox-active tyrosine proximal to the reactive iron center. We believe the differential residue conservation at position 121 for hydroxylases and halogenases is due to the isomeric flexibility of the reactive ferryl intermediate (**Fig 4B**).[14,15,35–37] Only one isomer of ferryl intermediate is plausible for hydroxylases: a trigonal bipyramidal structure with the oxo ligand and a histidine ligand defining the axial plane. Due to the presence of a third amino acid residue (Asp or Glu) coordinating to the iron center, the ferryl intermediate in hydroxylases is "locked" into one geometry. Even if a tyrosine ligand were present in the active site, so long as it's not proximal to the oxo ligand, unproductive oxidation to DOPA would not occur. Note that while all structures are drawn with succinate in monodentate coordination, bidentate coordination is also plausible. In halogenases, on the other hand, the Glu or Asp in the facial triad are replaced by Ala or Gly. This replacement sterically and

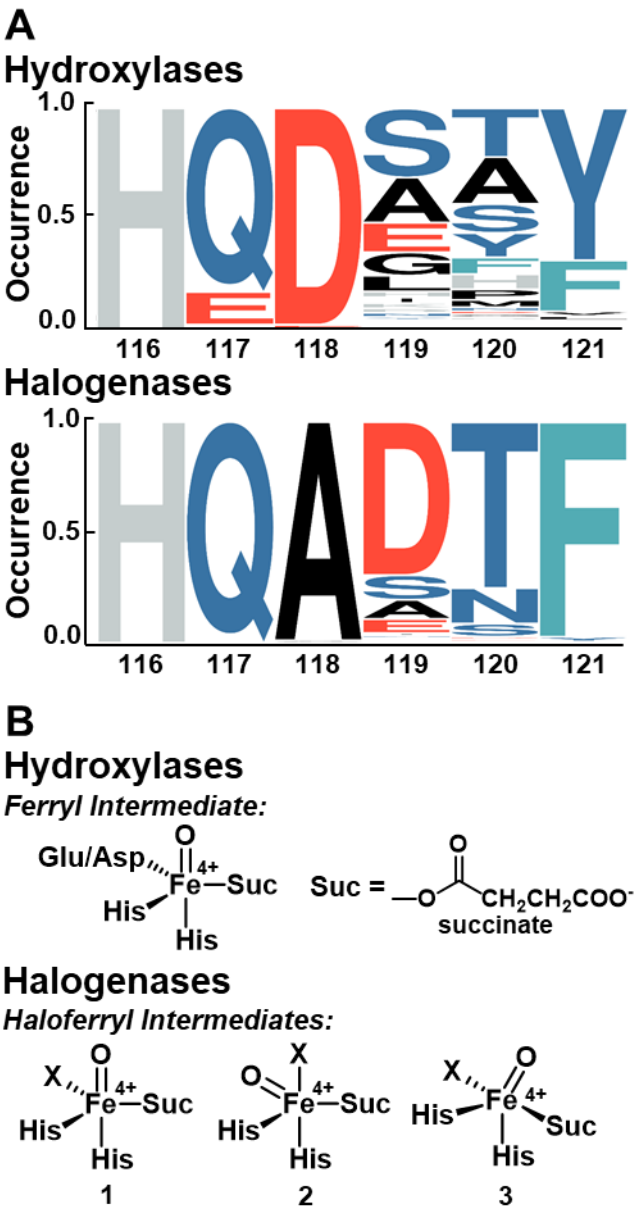

Figure 4. A) LOGOS plots displaying sequence conservations for homologues of SyrB2 for positions 116-121 in hydroxylases and halogenases. In halogenases, phenylalanine is strongly conserved at position 121. **B**) Potential reactive ferryl intermediates in hydroxylases and halogenases. X = halide.

electrostatically accommodates halide binding to the iron center. As a consequence, the protein's ability to "lock" the reactive intermediate into a single isomer is lost. Three different isomers for

the haloferryl intermediate have been proposed for halogenase systems (**Fig 4B**). One is analogous to hydroxylases and exists as trigonal bipyramidal structure with the oxo ligand and a histidine ligand defining the axial plane (**1**). Another isomer is structurally similar to **1** but swaps the positions of the oxo and halide ligands (**2**). The last isomer is best described as a heavily distorted trigonal bipyramidal structure, with the halide ligand and the coordinating oxygen of the succinate ligand defining the axial plane (**3**). Given this flexibility, any one of these intermediates could be reactive across the 2OG-dependent halogenase enzymes. Since reactive haloferryl intermediates exist in the timescales of hundreds of seconds, [11] halogenases must prevent a non-productive isomer from damaging the protein or leading to an unreactive enzyme intermediate. Evolution of the redox-inactive phenylalanine residue at position 121, therefore, prevents an unproductive oxidation from occurring, maintains catalytic activity, and allows the halogenase to align a productive ferryl isomer for its halogenation function.

Conclusions

We show that the incorporation of a redox active tyrosine residue at position 121 in SyrB2 results in further post-translational modification to DOPA. This DOPA residue binds ferric iron with very high affinity and results in a catalytically inactive, off-cycle enzymatic species. The ferric-DOPA species likely forms as a result of an unproductive oxidation in F121Y-SyrB2 (**Scheme 1**). After H-atom abstraction of the hydroxyl group of Y121, the newly formed hydroxyl group on the iron center will rebound and incorporate into the ring structure, eventually forming DOPA121. This residue can become deprotonated and bind ferric iron from the cellular environment, forming the blue-green chromophore we observe upon purification of this protein (**Fig. 1B**). To avoid such unproductive oxidations, halogenases tend to keep redox-inactive residues in their SCS, especially in position 121. The placement of redox-inactive residues in the

halogenases is especially important due to multiple isomers of ferryl intermediates, as compared to the hydroxylases. This study also explores the function of H-bonding in the active sites of halogenases, and their implications on catalysis. Our results serve as a warning to others attempting to engineer non-heme iron enzymes for non-native functions,[38–40] as placement of redox-active residues can result in catalytically non-functional enzymes.

Scheme 1. Proposed reaction mechanism for the formation of DOPA121 in SyrB2.

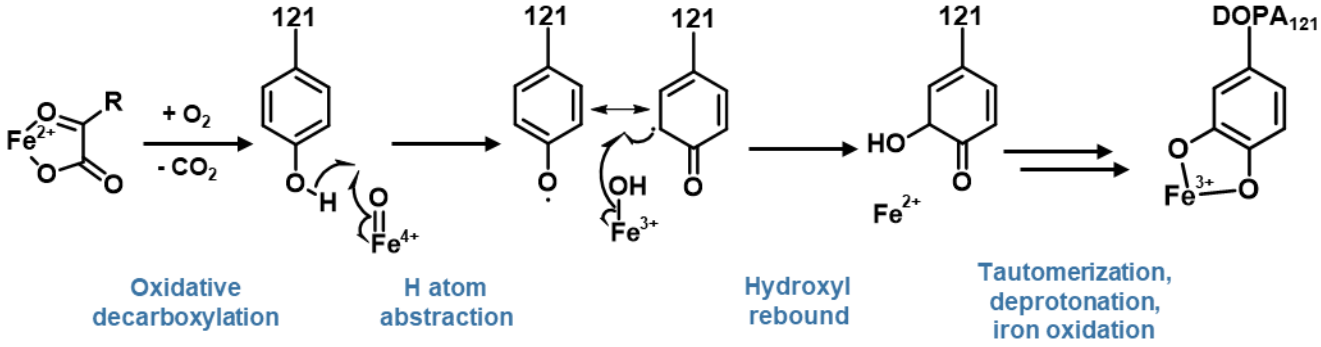

ASSOCIATED CONTENT

Supporting Information.

Supporting Information is available free of charge via the Internet at DOI:_____

AUTHOR INFORMATION

Corresponding Author

*ambikab@umn.edu

Author Contributions

ABD conceived the idea and supervised the project. RHW designed and synthesized the proteins, and performed the various biochemical, and analytical studies on them. RHW, SC, ERS, JJD designed and performed the LC-MS based halogenation assay.

RHW and ERS performed bioinformatics studies. RHW and ABD wrote the manuscript with contributions from all authors. All authors have given approval to the final version of the manuscript.

Funding Sources

RHW and ERS acknowledge the support of the National Institute of Health Chemical Biology Training Grant (T32GM132029). This work was supported by the Regents of the University of Minnesota and National Science Foundation CLP and CBET (grant #2046527).

ACKNOWLEDGMENT

The authors would like to thank Dr. Rahul Banerjee and Prof. John Lipscomb for their productive discussions for EPR experiments. We also thank Prof. William Pomerantz and Noelle Olsen for sodium molybdate dihydrate for the DOPA nitration/oxidation assays. Authors thank Profs. Bollinger and Krebs (Penn State) for SyrB1, SyrB2, and Sfp plasmids and Prof. Blaskus (Harvard) for TycF plasmid.

ABBREVIATIONS

2OG, 2-oxoglutarate; SCS, secondary coordination sphere; DOPA, dihydroxyphenylalanine; LMCT, ligand-to-metal charge transfer; Ppt, phosphopantetheine; AQC, 6-aminoquinolyl-N-hydroxysuccinimidyl carbamate

REFERENCES

(1) Kal, S.; Que, L. Dioxygen Activation by Nonheme Iron Enzymes with the 2-His-1-Carboxylate Facial Triad That Generate High-Valent Oxoiron Oxidants. *JBIC J. Biol. Inorg. Chem.* **2017**, *22* (2–3), 339–365. https://doi.org/10.1007/s00775-016-1431-2.

(2) Lee, H.-J.; Lloyd, M. D.; Harlos, K.; Clifton, I. J.; Baldwin, J. E.; Schofield, C. J. Kinetic and Crystallographic Studies on Deacetoxycephalosporin C Synthase (DAOCS)11Edited by R. Huber. *J. Mol. Biol.* **2001**, *308* (5), 937–948. https://doi.org/10.1006/jmbi.2001.4649.

(3) Hirsilä, M.; Koivunen, P.; Günzler, V.; Kivirikko, K. I.; Myllyharju, J. Characterization of the Human Prolyl 4-Hydroxylases That Modify the Hypoxia-Inducible Factor*. *J. Biol. Chem.* **2003**, *278* (33), 30772–30780. https://doi.org/10.1074/jbc.M304982200.

(4) Hegg, E. L.; Jr, L. Q. The 2-His-1-Carboxylate Facial Triad — An Emerging Structural Motif in Mononuclear Non-Heme Iron(II) Enzymes. *Eur. J. Biochem.* **1997**, *250* (3), 625–629. https://doi.org/10.1111/j.1432-1033.1997.t01-1-00625.x.
(5) Blasiak, L. C.; Vaillancourt, F. H.; Walsh, C. T.; Drennan, C. L. Crystal Structure of the Non-Haem Iron Halogenase SyrB2 in Syringomycin Biosynthesis. *Nature* **2006**, *440* (7082), 368–371. https://doi.org/10.1038/nature04544.
(6) Solomon, E. I.; Goudarzi, S.; Sutherlin, K. D. O2 Activation by Non-Heme Iron Enzymes. *Biochemistry* **2016**, *55* (46), 6363–6374. https://doi.org/10.1021/acs.biochem.6b00635.
(7) Solomon, E. I.; DeWeese, D. E.; Babicz, J. T. Mechanisms of O2 Activation by Mononuclear Non-Heme Iron Enzymes. *Biochemistry* **2021**, *60* (46), 3497–3506. https://doi.org/10.1021/acs.biochem.1c00370.
(8) Vaillancourt, F. H.; Yin, J.; Walsh, C. T. SyrB2 in Syringomycin E Biosynthesis Is a Nonheme FeII α-Ketoglutarate- and O2-Dependent Halogenase. *Proc. Natl. Acad. Sci.* **2005**, *102* (29), 10111–10116. https://doi.org/10.1073/pnas.0504412102.
(9) Vaillancourt, F. H.; Vosburg, D. A.; Walsh, C. T. Dichlorination and Bromination of a Threonyl-S-Carrier Protein by the Non-Heme FeII Halogenase SyrB2. *ChemBioChem* **2006**, *7* (5), 748–752. https://doi.org/10.1002/cbic.200500480.
(10) Matthews, M. L.; Neumann, C. S.; Miles, L. A.; Grove, T. L.; Booker, S. J.; Krebs, C.; Walsh, C. T.; Bollinger, J. M. Substrate Positioning Controls the Partition between Halogenation and Hydroxylation in the Aliphatic Halogenase, SyrB2. *Proc. Natl. Acad. Sci.* **2009**, *106* (42), 17723–17728. https://doi.org/10.1073/pnas.0909649106.
(11) Matthews, M. L.; Krest, C. M.; Barr, E. W.; Vaillancourt, F. H.; Walsh, C. T.; Green, M. T.; Krebs, C.; Bollinger, J. M. Substrate-Triggered Formation and Remarkable Stability of the C−H Bond-Cleaving Chloroferryl Intermediate in the Aliphatic Halogenase, SyrB2. *Biochemistry* **2009**, *48* (20), 4331–4343. https://doi.org/10.1021/bi900109z.
(12) Kulik, H. J.; Drennan, C. L. Substrate Placement Influences Reactivity in Non-Heme Fe(II) Halogenases and Hydroxylases *. *J. Biol. Chem.* **2013**, *288* (16), 11233–11241. https://doi.org/10.1074/jbc.M112.415570.
(13) Martinie, R. J.; Livada, J.; Chang, W.; Green, M. T.; Krebs, C.; Bollinger, J. M.; Silakov, A. Experimental Correlation of Substrate Position with Reaction Outcome in the Aliphatic Halogenase, SyrB2. *J. Am. Chem. Soc.* **2015**, *137* (21), 6912–6919. https://doi.org/10.1021/jacs.5b03370.
(14) Mehmood, R.; Qi, H. W.; Steeves, A. H.; Kulik, H. J. The Protein's Role in Substrate Positioning and Reactivity for Biosynthetic Enzyme Complexes: The Case of SyrB2/SyrB1. *ACS Catal.* **2019**, *9* (6), 4930–4943. https://doi.org/10.1021/acscatal.9b00865.
(15) Rugg, G.; M. Senn, H. Formation and Structure of the Ferryl [Fe[Double Bond, Length as m-Dash]O] Intermediate in the Non-Haem Iron Halogenase SyrB2: Classical and QM/MM Modelling Agree. *Phys. Chem. Chem. Phys.* **2017**, *19* (44), 30107–30119. https://doi.org/10.1039/C7CP05937J.
(16) Mitchell, A. J.; Zhu, Q.; Maggiolo, A. O.; Ananth, N. R.; Hillwig, M. L.; Liu, X.; Boal, A. K. Structural Basis for Halogenation by Iron- and 2-Oxo-Glutarate-Dependent Enzyme WelO5. *Nat. Chem. Biol.* **2016**, *12* (8), 636–640. https://doi.org/10.1038/nchembio.2112.
(17) Zhang, X.; Wang, Z.; Gao, J.; Liu, W. Chlorination versus Hydroxylation Selectivity Mediated by the Non-Heme Iron Halogenase WelO5. *Phys. Chem. Chem. Phys.* **2020**, *22* (16), 8699–8712. https://doi.org/10.1039/D0CP00791A.

(18) Neugebauer, M. E.; Sumida, K. H.; Pelton, J. G.; McMurry, J. L.; Marchand, J. A.; Chang, M. C. Y. A Family of Radical Halogenases for the Engineering of Amino-Acid-Based Products. *Nat. Chem. Biol.* **2019**, *15* (10), 1009–1016. https://doi.org/10.1038/s41589-019-0355-x.

(19) Bhagi-Damodaran, A.; Reed, J. H.; Zhu, Q.; Shi, Y.; Hosseinzadeh, P.; Sandoval, B. A.; Harnden, K. A.; Wang, S.; Sponholtz, M. R.; Mirts, E. N.; Dwaraknath, S.; Zhang, Y.; Moënne-Loccoz, P.; Lu, Y. Heme Redox Potentials Hold the Key to Reactivity Differences between Nitric Oxide Reductase and Heme-Copper Oxidase. *Proc. Natl. Acad. Sci.* **2018**, *115* (24), 6195–6200. https://doi.org/10.1073/pnas.1720298115.

(20) Bhagi-Damodaran, A.; Petrik, I. D.; Marshall, N. M.; Robinson, H.; Lu, Y. Systematic Tuning of Heme Redox Potentials and Its Effects on O2 Reduction Rates in a Designed Oxidase in Myoglobin. *J. Am. Chem. Soc.* **2014**, *136* (34), 11882–11885. https://doi.org/10.1021/ja5054863.

(21) Gasteiger, E.; Hoogland, C.; Gattiker, A.; Duvaud, S.; Wilkins, M. R.; Appel, R. D.; Bairoch, A. Protein Identification and Analysis Tools on the ExPASy Server. In *The Proteomics Protocols Handbook*; Walker, J. M., Ed.; Humana Press: Totowa, NJ, 2005; pp 571–607. https://doi.org/10.1385/1-59259-890-0:571.

(22) Waite, J. H.; Benedict, C. V. Assay of Dihydroxyphenylalanine (Dopa) in Invertebrate Structural Proteins. In *Methods in Enzymology*; Posttranslational Modifications Part B; Academic Press, 1984; Vol. 107, pp 397–413. https://doi.org/10.1016/0076-6879(84)07028-2.

(23) Farquhar, E. R.; Emerson, J. P.; Koehntop, K. D.; Reynolds, M. F.; Trmčić, M.; Que, L. In Vivo Self-Hydroxylation of an Iron-Substituted Manganese-Dependent Extradiol Cleaving Catechol Dioxygenase. *JBIC J. Biol. Inorg. Chem.* **2011**, *16* (4), 589–597. https://doi.org/10.1007/s00775-011-0760-4.

(24) Liu, A.; Ho, R. Y. N.; Que, L.; Ryle, M. J.; Phinney, B. S.; Hausinger, R. P. Alternative Reactivity of an α-Ketoglutarate-Dependent Iron(II) Oxygenase: Enzyme Self-Hydroxylation. *J. Am. Chem. Soc.* **2001**, *123* (21), 5126–5127. https://doi.org/10.1021/ja005879x.

(25) Liu, P.; Mehn, M. P.; Yan, F.; Zhao, Z.; Que, Lawrence; Liu, H. Oxygenase Activity in the Self-Hydroxylation of (S)-2-Hydroxypropylphosphonic Acid Epoxidase Involved in Fosfomycin Biosynthesis. *J. Am. Chem. Soc.* **2004**, *126* (33), 10306–10312. https://doi.org/10.1021/ja0475050.

(26) Ryle, M. J.; Koehntop, K. D.; Liu, A.; Que, L.; Hausinger, R. P. Interconversion of Two Oxidized Forms of Taurine/α-Ketoglutarate Dioxygenase, a Non-Heme Iron Hydroxylase: Evidence for Bicarbonate Binding. *Proc. Natl. Acad. Sci.* **2003**, *100* (7), 3790–3795. https://doi.org/10.1073/pnas.0636740100.

(27) Solomon, E. I.; Brunold, T. C.; Davis, M. I.; Kemsley, J. N.; Lee, S.-K.; Lehnert, N.; Neese, F.; Skulan, A. J.; Yang, Y.-S.; Zhou, J. Geometric and Electronic Structure/Function Correlations in Non-Heme Iron Enzymes. *Chem. Rev.* **2000**, *100* (1), 235–350. https://doi.org/10.1021/cr9900275.

(28) Whittaker, J. W.; Lipscomb, J. D.; Kent, T. A.; Münck, E. Brevibacterium Fuscum Protocatechuate 3,4-Dioxygenase. Purification, Crystallization, and Characterization. *J. Biol. Chem.* **1984**, *259* (7), 4466–4475. https://doi.org/10.1016/S0021-9258(17)43071-7.

(29) Bradley, F. C.; Lindstedt, S.; Lipscomb, J. D.; Que, L.; Roe, A. L.; Rundgren, M. 4-Hydroxyphenylpyruvate Dioxygenase Is an Iron-Tyrosinate Protein. *J. Biol. Chem.* **1986**, *261* (25), 11693–11696. https://doi.org/10.1016/S0021-9258(18)67299-0.
(30) Miller, M. A.; Lipscomb, J. D. Homoprotocatechuate 2,3-Dioxygenase from Brevibacterium Fuscum: A DIOXYGENASE WITH CATALASE ACTIVITY. *J. Biol. Chem.* **1996**, *271* (10), 5524–5535. https://doi.org/10.1074/jbc.271.10.5524.
(31) Taylor, S. W.; Chase, D. B.; Emptage, M. H.; Nelson, M. J.; Waite, J. H. Ferric Ion Complexes of a DOPA-Containing Adhesive Protein from Mytilus Edulis. *Inorg. Chem.* **1996**, *35* (26), 7572–7577. https://doi.org/10.1021/ic960514s.
(32) Ormö, M.; deMaré, F.; Regnström, K.; Aberg, A.; Sahlin, M.; Ling, J.; Loehr, T. M.; Sanders-Loehr, J.; Sjöberg, B. M. Engineering of the Iron Site in Ribonucleotide Reductase to a Self-Hydroxylating Monooxygenase. *J. Biol. Chem.* **1992**, *267* (13), 8711–8714. https://doi.org/10.1016/S0021-9258(19)50335-0.
(33) Albe, K. R.; Butler, M. H.; Wright, B. E. Cellular Concentrations of Enzymes and Their Substrates. *J. Theor. Biol.* **1990**, *143* (2), 163–195. https://doi.org/10.1016/S0022-5193(05)80266-8.
(34) Yeh, E.; Kohli, R. M.; Bruner, S. D.; Walsh, C. T. Type II Thioesterase Restores Activity of a NRPS Module Stalled with an Aminoacyl-S-Enzyme That Cannot Be Elongated. *ChemBioChem* **2004**, *5* (9), 1290–1293. https://doi.org/10.1002/cbic.200400077.
(35) Huang, J.; Li, C.; Wang, B.; Sharon, D. A.; Wu, W.; Shaik, S. Selective Chlorination of Substrates by the Halogenase SyrB2 Is Controlled by the Protein According to a Combined Quantum Mechanics/Molecular Mechanics and Molecular Dynamics Study. *ACS Catal.* **2016**, *6* (4), 2694–2704. https://doi.org/10.1021/acscatal.5b02825.
(36) Wong, S. D.; Srnec, M.; Matthews, M. L.; Liu, L. V.; Kwak, Y.; Park, K.; Bell III, C. B.; Alp, E. E.; Zhao, J.; Yoda, Y.; Kitao, S.; Seto, M.; Krebs, C.; Bollinger, J. M.; Solomon, E. I. Elucidation of the Fe(Iv)=O Intermediate in the Catalytic Cycle of the Halogenase SyrB2. *Nature* **2013**, *499* (7458), 320–323. https://doi.org/10.1038/nature12304.
(37) Srnec, M.; Wong, S. D.; Matthews, M. L.; Krebs, C.; Bollinger, J. M.; Solomon, E. I. Electronic Structure of the Ferryl Intermediate in the α-Ketoglutarate Dependent Non-Heme Iron Halogenase SyrB2: Contributions to H Atom Abstraction Reactivity. *J. Am. Chem. Soc.* **2016**, *138* (15), 5110–5122. https://doi.org/10.1021/jacs.6b01151.
(38) Neugebauer, M. E.; Kissman, E. N.; Marchand, J. A.; Pelton, J. G.; Sambold, N. A.; Millar, D. C.; Chang, M. C. Y. Reaction Pathway Engineering Converts a Radical Hydroxylase into a Halogenase. *Nat. Chem. Biol.* **2021**, 1–9. https://doi.org/10.1038/s41589-021-00944-x.
(39) Goldberg, N. W.; Knight, A. M.; Zhang, R. K.; Arnold, F. H. Nitrene Transfer Catalyzed by a Non-Heme Iron Enzyme and Enhanced by Non-Native Small-Molecule Ligands. *J. Am. Chem. Soc.* **2019**, *141* (50), 19585–19588. https://doi.org/10.1021/jacs.9b11608.
(40) Mitchell, A. J.; Dunham, N. P.; Bergman, J. A.; Wang, B.; Zhu, Q.; Chang, W.; Liu, X.; Boal, A. K. Structure-Guided Reprogramming of a Hydroxylase To Halogenate Its Small Molecule Substrate. *Biochemistry* **2017**, *56* (3), 441–444. https://doi.org/10.1021/acs.biochem.6b01173.

SUPPLEMENTARY INFORMATION

Role of a secondary coordination sphere residue in halogenation catalysis of non-heme iron enzymes

*R. Hunter Wilson, Sourav Chatterjee, Elizabeth R. Smithwick, Joseph J. Dalluge, Ambika Bhagi-Damodaran**

Department of Chemistry, University of Minnesota, Twin Cities, Minneapolis, MN 55455, USA

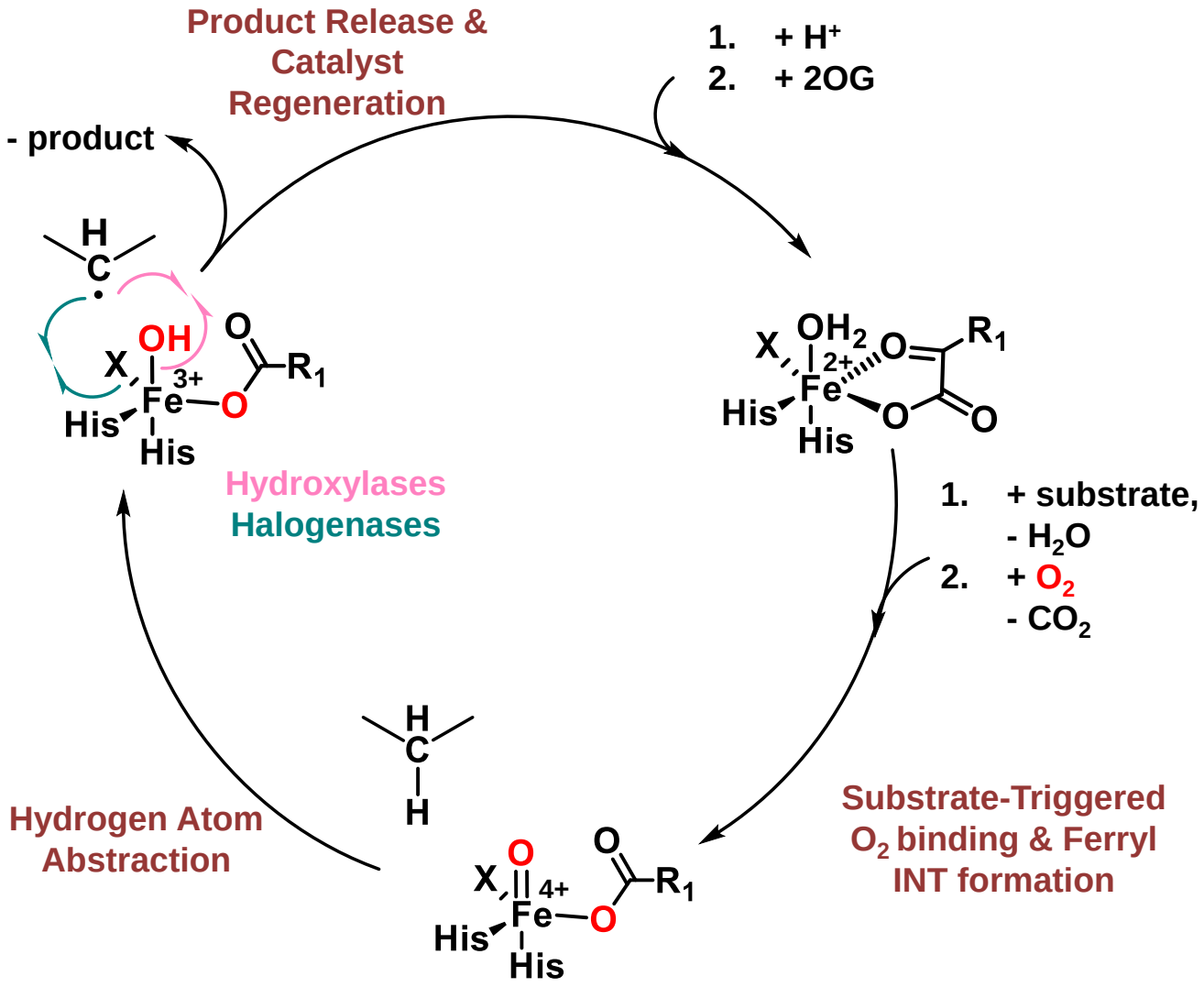

Figure S1. Catalytic Cycle for 2OG-dependent hydroxylases and halogenases. X = Asp/Glu in hydroxylases; X = Cl^-/Br^- in halogenases. The protein binds ferrous iron and 2OG to enter the resting state. Upon substrate binding, a water molecule is displaced, and oxygen binding is triggered. An oxidative decarboxylation occurs, breaking the O-O bond of oxygen, and forming the reactive ferryl intermediate. The ferryl intermediate abstracts a hydrogen atom from the substrate forming a substrate radical. In hydroxylases, the hydroxide ligand will rebound with the substrate radical and form a hydroxylated species. In halogenases, the enzyme positions the halide proximal to the substrate to favor forming a halogenated product via a similar radical mechanism. Arrow indicating single electron flow back to iron omitted; the result in both pathways is a reduction of the ferric iron to a ferrous state. Following product release, the enzyme can bind 2OG again and restart the catalytic cycle.

Table S1. SRM transitions monitored for UPLC-MS/MS detection of threonine and enzymatically modified threonines.

Compound	SRM Transition	Cone (V)	Collision Energy (eV)
AQC-Threonine	290.2>171.1	35	20
AQC-OH-Threonine	306.2>171.1	35	20
AQC-Cl-Threonine	324.1>171.1	35	20
AQC-^{37}Cl-Threonine	326.1>171.1	35	20

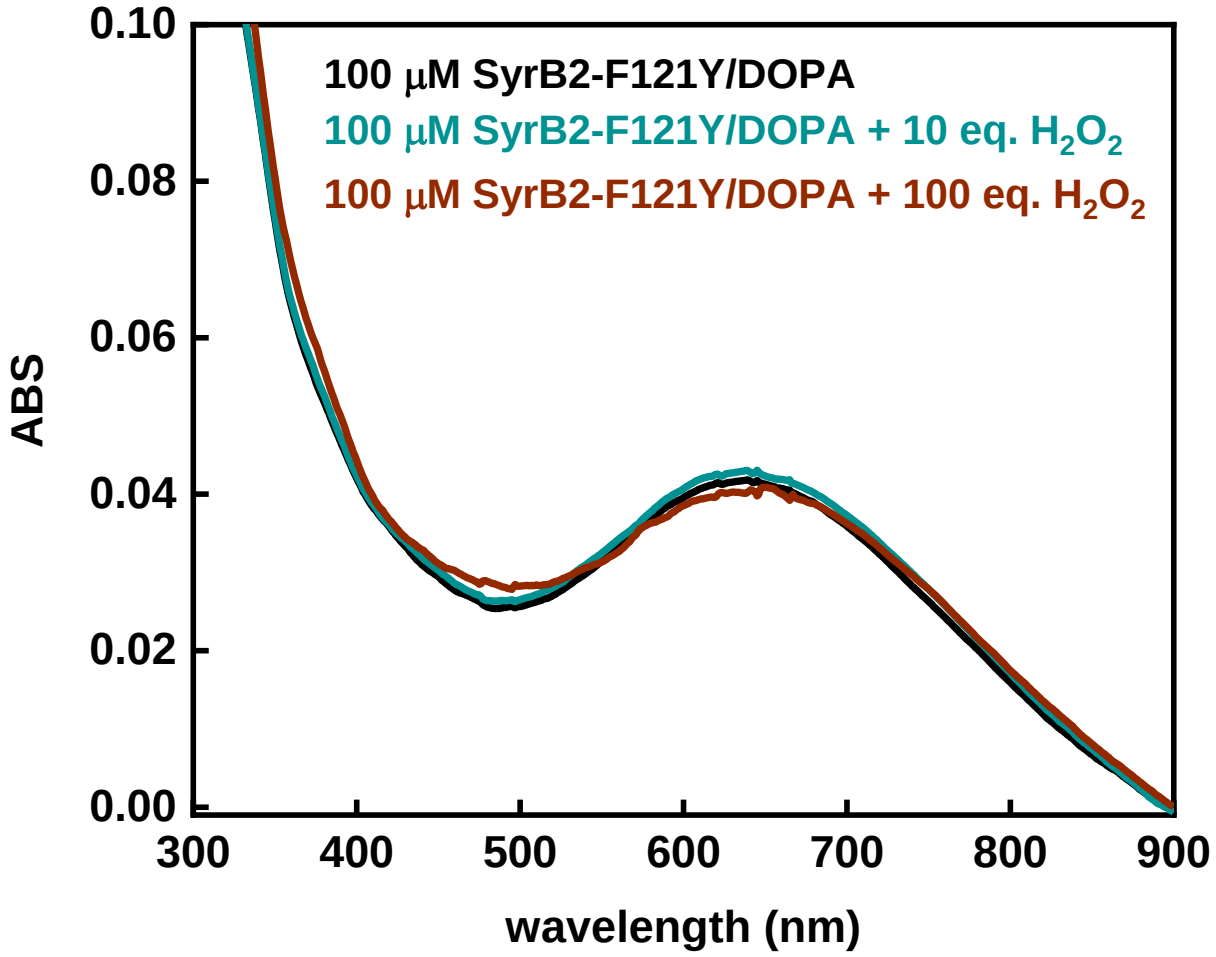

Figure S2. UV-Vis spectra of 100 μM SyrB2-F121Y/DOPA mixed with varying amounts of hydrogen peroxide. Since no spectral shift is observed with any of the samples, assignment of a ferrous state would be incorrect. The protein was purified aerobically so it's most likely the chromophore's generated with a ferric iron center. Spectrum background corrected at 900 nm.

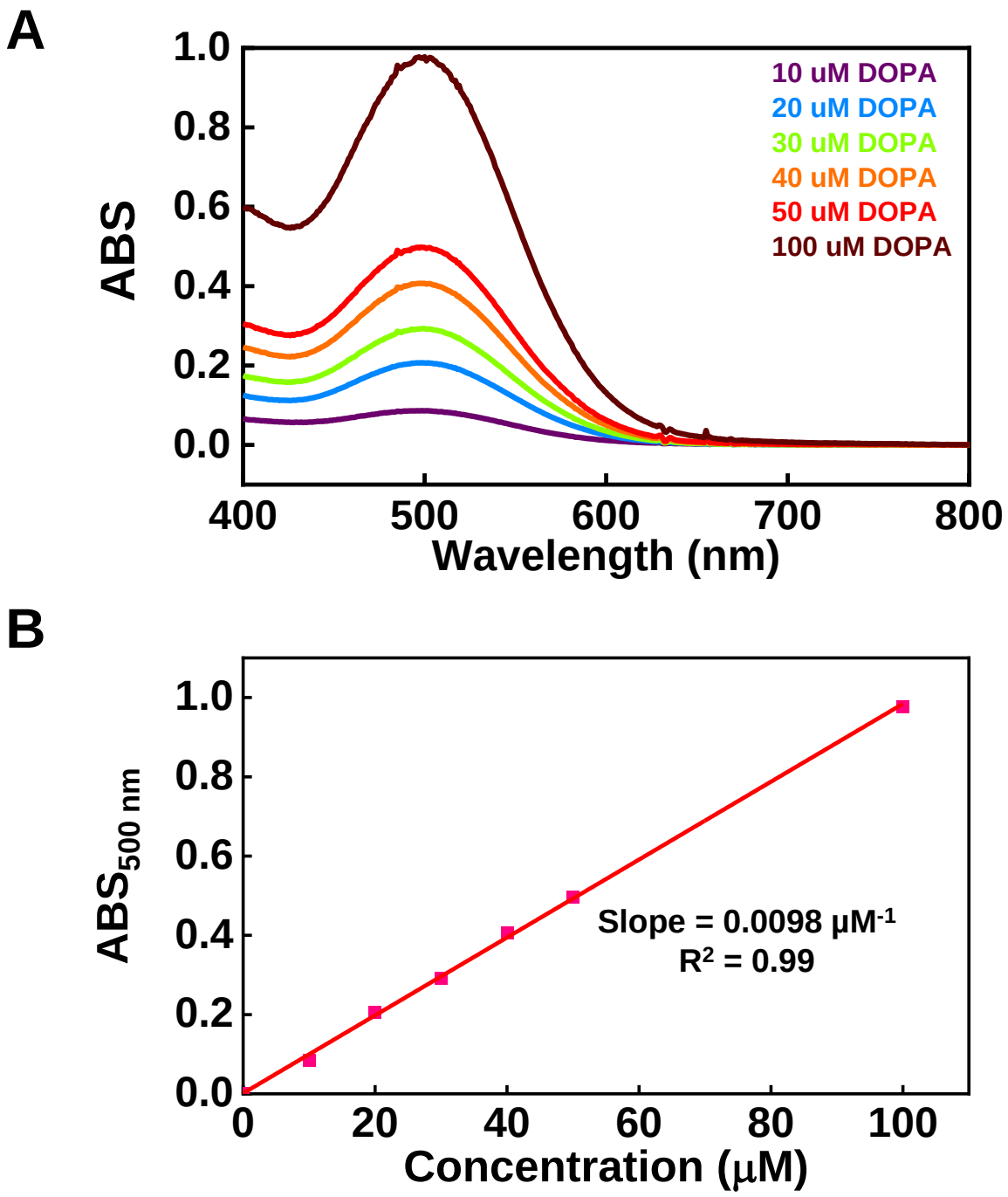

Figure S3. A) UV-Vis spectra of products from a DOPA-specific nitration/oxidation reaction using various concentrations of L-DOPA. Reactant concentrations of L-DOPA are provided in the inset. **B**) Standard curve of the dinitro-L-DOPA-quinone product using the absorbance at λ_{max} 500 nm.

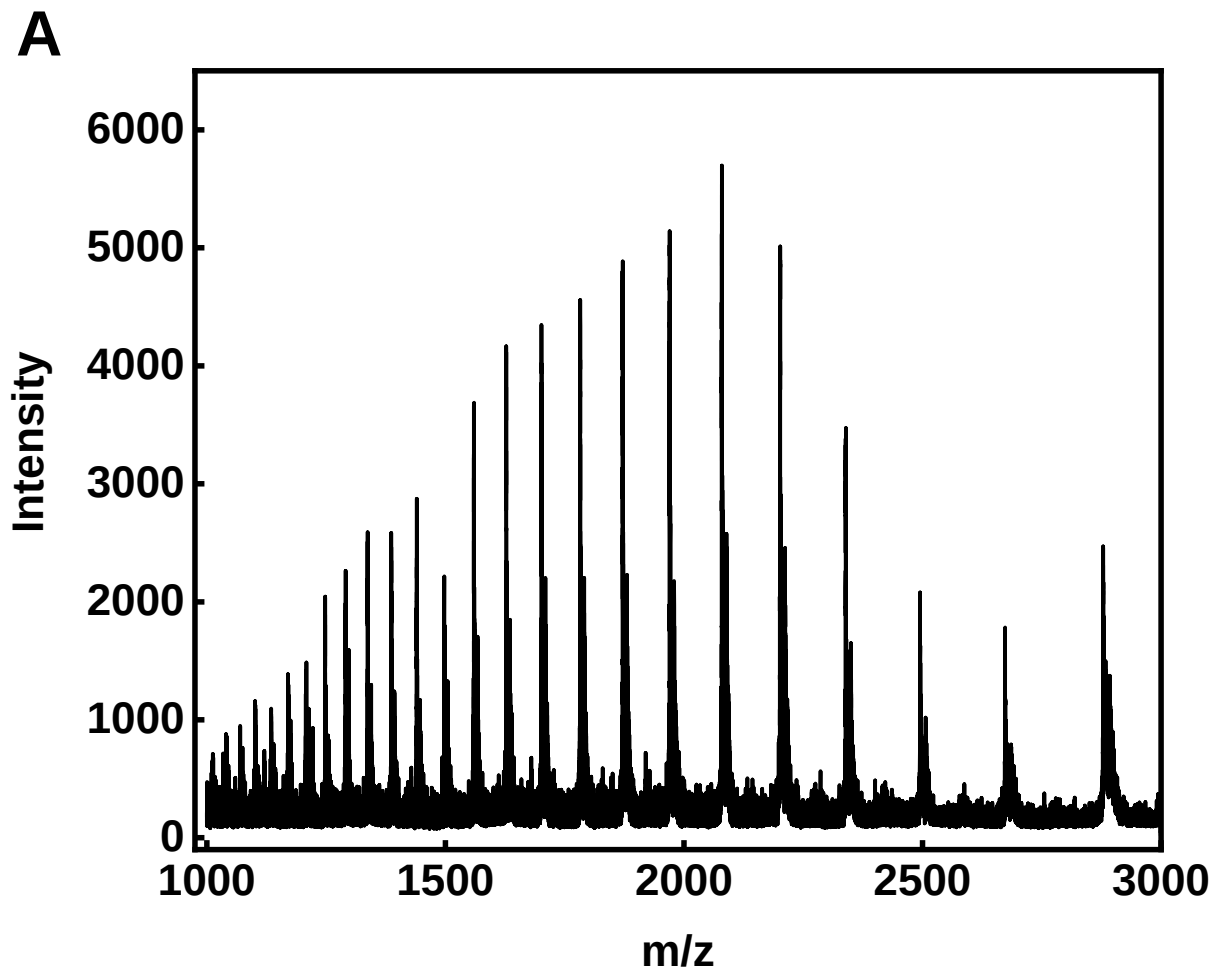

Figure S4. A) Complete mass spectrum of the F121Y/DOPA protein displaying multiple charge states for the two species.

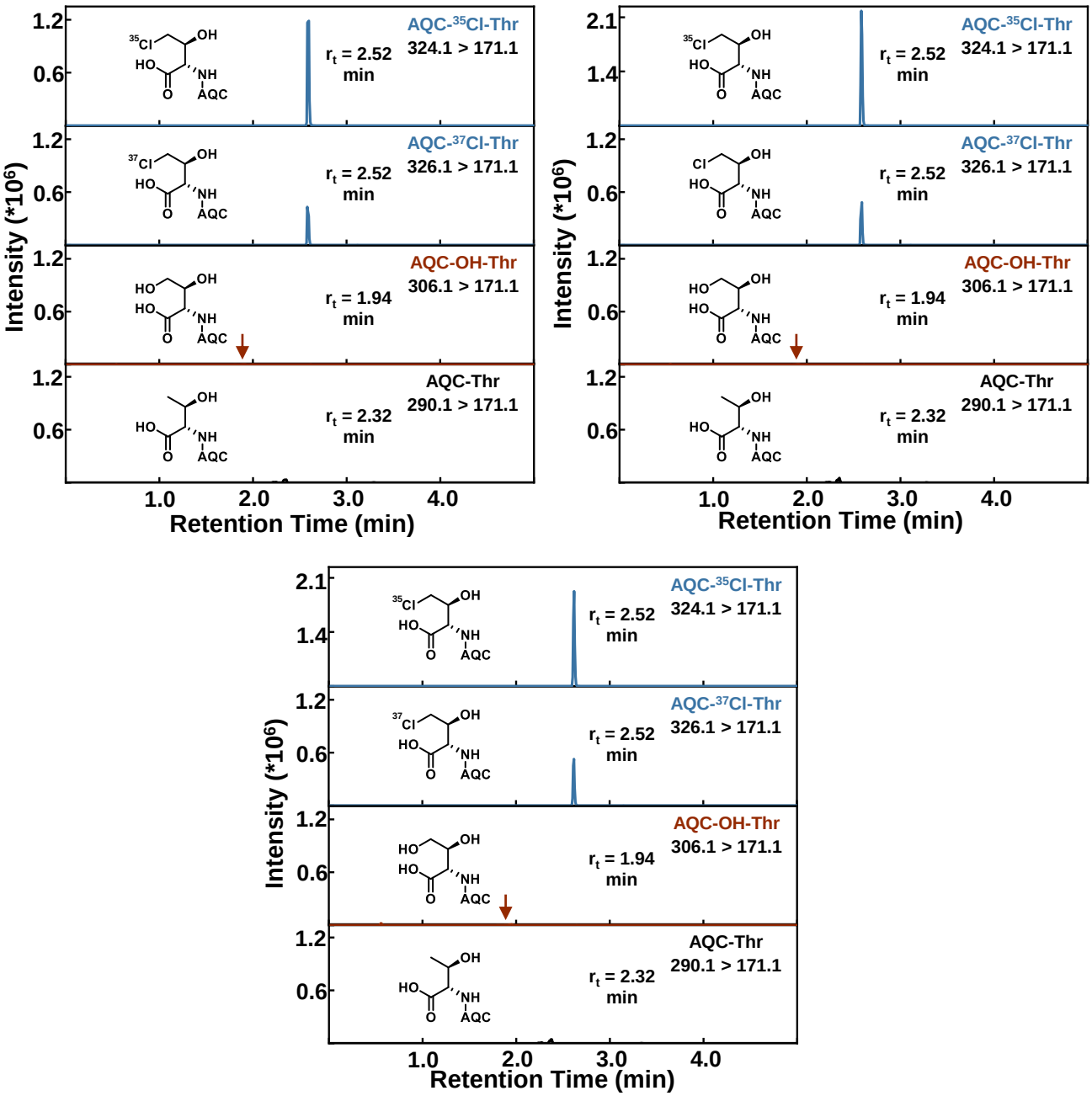

Figure S5. UPLC-MRM-MS/MS chromatograms of the halogenation reaction products using the WT SyrB2 protein. Mass transitions for each unique analyte are given in the top right of each chromatogram.

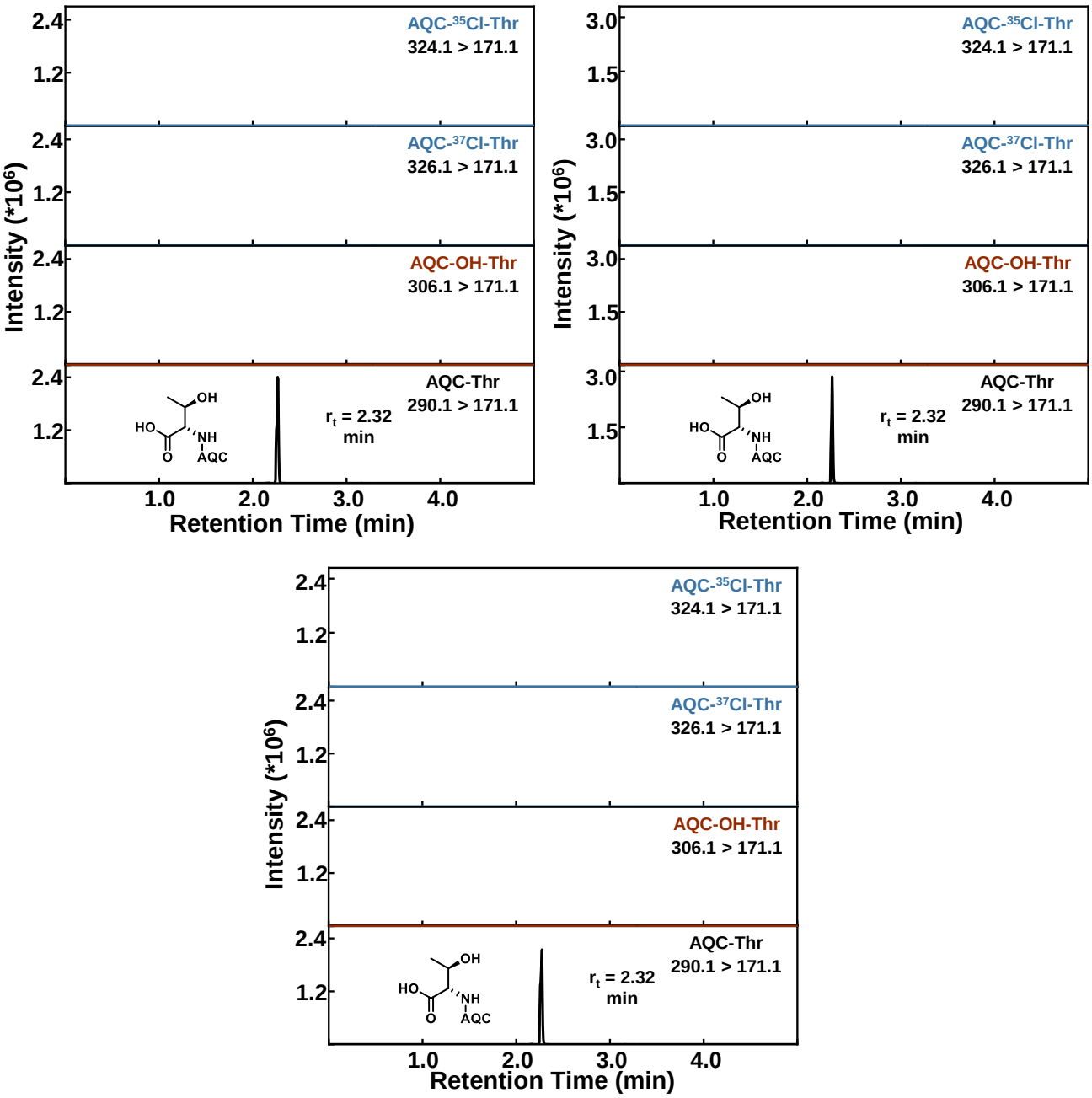

Figure S6. UPLC-MRM-MS/MS chromatograms of the halogenation reaction products using the F121Y/DOPA SyrB2 protein. Mass transitions for each unique analyte are given in the top right of each chromatogram.

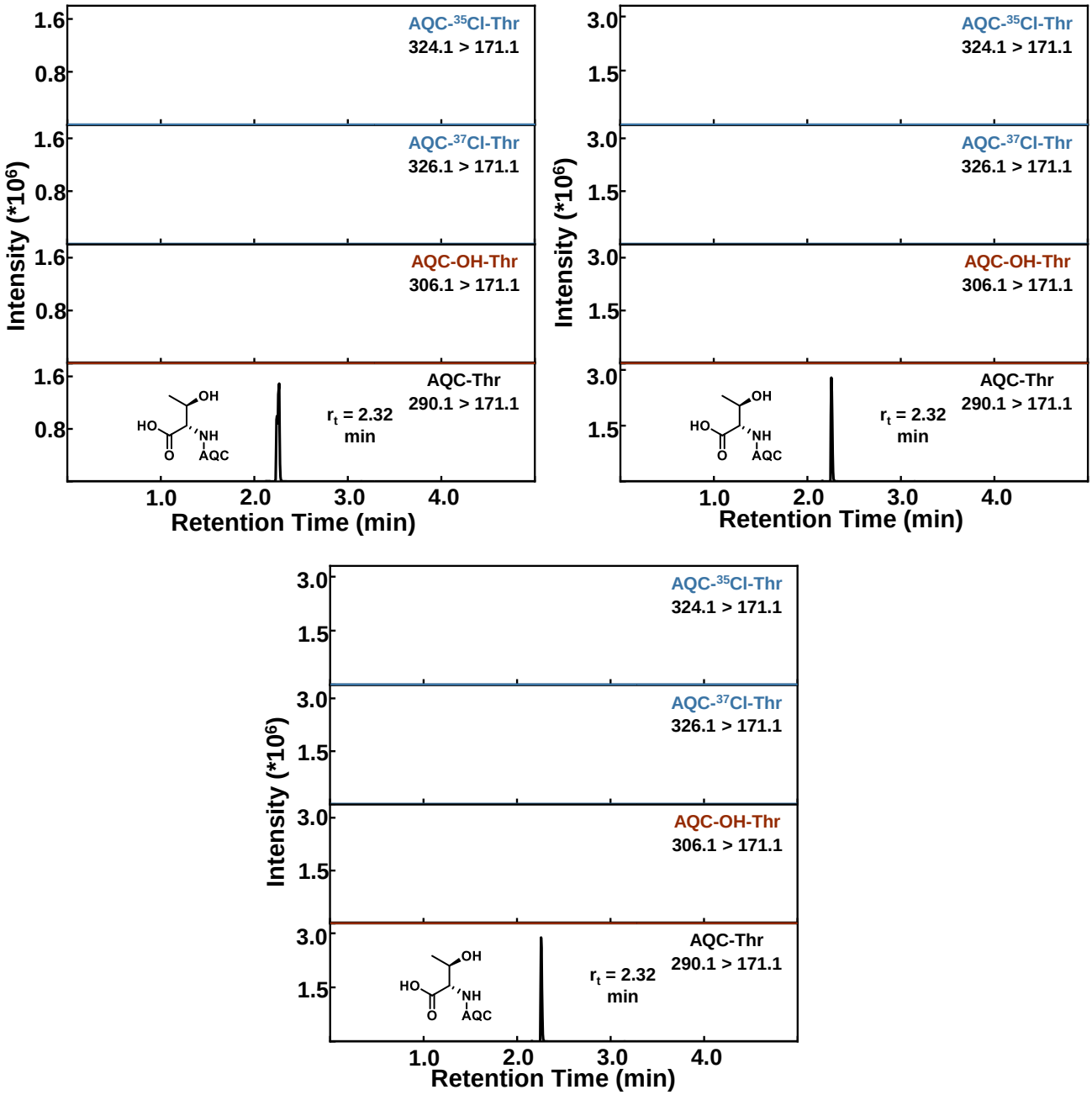

Figure S7. UPLC-MRM-MS/MS chromatograms of the halogenation reaction products using the F121Y/DOPA SyrB2 protein and 10 eq. of sodium ascorbate reductant. Mass transitions for each unique analyte are given in the top right of each chromatogram.

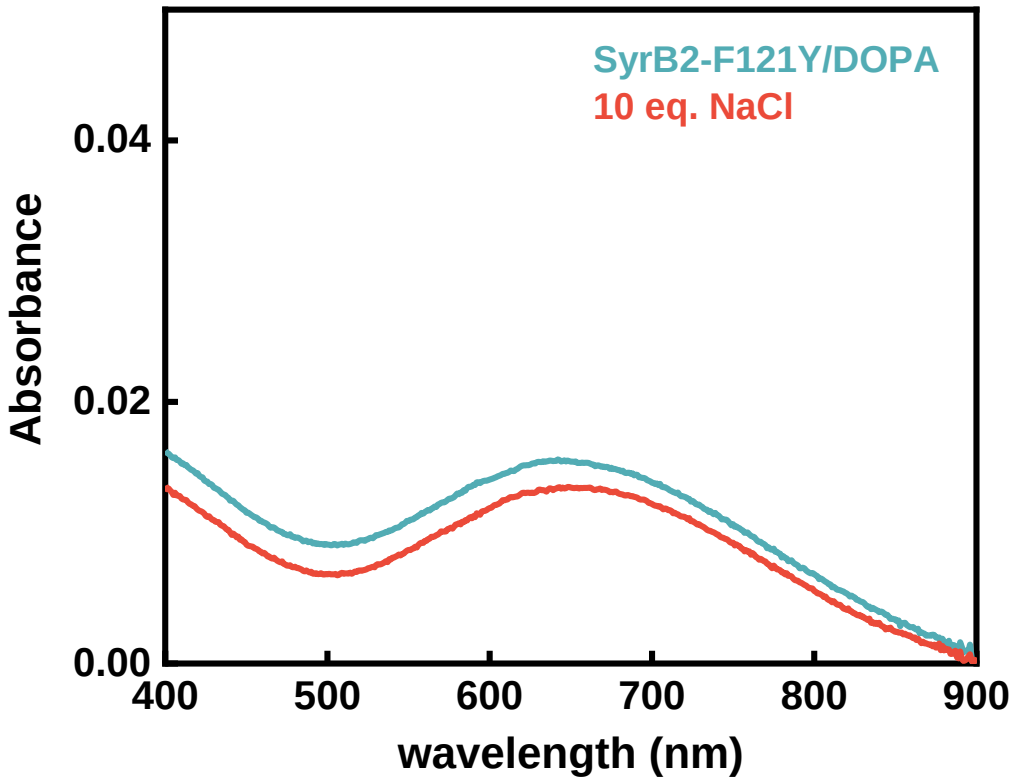

Figure S8. UV-Vis spectra of SyrB2-F121Y/DOPA (75 µM) before and after the addition of 10 eq. NaCl. No discernable shift in the UV-spectrum is observed implying that DOPA is occupying the halide binding position.